❒      2143

# Autism spectrum disorder identification with multi-site functional magnetic resonance imaging

**Shabeena Lylath, Laxmi B. Rananavare**

Department of Computer Science and Engineering, Reva University, Bangalore, India

## Article Info

## ABSTRACT

Autism spectrum disorder (ASD) is a neurodevelopmental condition characterized by enduring difficulties in social interaction and communication. People analyzed with ASD may display repetitive behaviors and limited interests. Autism is classified as a spectrum disorder, implying that the symptom intensity might range from mild to severe depending on the individual. To detect ASD in this paper an attribute feature graph approach is designed by using the stastical dependencies features that necessarily accomplish the diagnosis of ASD. In the first phase the features extracted are designed based on the functional magnetic resonance imaging (fMRI) data, in the next-step the attribute feature graph layer learns the features of the node information of various nodes by ASD classification. Further, in the third step, it is employed to independently extract distinguishing features from the functional connectivity matrices of the brain that are derived from fMRI. The custom convolutional neural network (CNN) used in this study is trained on a comprehensive dataset comprising individuals diagnosed with ASD and typically developing individuals. In the fourth stage, a prototype learning is developed to augment the classification performance of the custom-CNN. The experimental analysis further carried out states that the proposed model works efficiently in comparison with the existing system.

## Corresponding Author:

Shabeena Lylath
Department of Computer Science and Engineering, Reva University
Bangalore, India
Email: shabeenal_12@rediffmail.com

## 1. INTRODUCTION

Autism spectrum disorder (ASD) is a neurodevelopmental disease that has detrimental effects on early brain development and an individual's capacity for social interaction [1]. ASD is characterized by the presence of restrictive and repetitive behavioral patterns. The term "spectrum" encompasses a diverse range of symptoms that vary in their level of severity [2]. Although there is currently no established treatment for ASD, early intervention and appropriate medical care have the potential to significantly improve a child's development by enhancing their behavioral and communicative skills [3]. Identifying and diagnosing ASD through standard behavioral investigations pose significant challenges and complexities. Autism may be diagnosed beyond the typical age of two, depending on it is severity [4]. There exist multiple accessible treatment strategies that can be employed to detect ASD at the earliest possible stage. Diagnostic procedures are typically not extensively utilized until a child is deemed to have a high risk of developing autism.

The diagnosis of ASD is typically made in children aged 48 to 60 months, indicating a delay of two years [5]. Most children are typically not diagnosed with ASD until they reach the age of 48 to 60 months. This is the case even though there are observable signs of ASD as early as 12 months, and there is a

possibility of diagnosis by 18 months [6]. The diagnostic delay of 12 to 14 months has an impact on early intervention programs, which have the potential to increase children's IQs by 10 to 15 points if initiated before the age of three [7]. In order to enhance the quality of life for children diagnosed with ASD, it is imperative to prioritize early diagnosis and treatment for ASD.

Magnetic resonance imaging (MRI) and positron emission tomography (PET) are commonly utilized neuroimaging techniques for investigating the neurodevelopmental characteristics associated with ASD [8]. In recent decades, there has been a notable increase in research dedicated to investigating structural and functional brain abnormalities that may serve as indicators of ASD. The neurodevelopmental characteristics of ASD have been extensively studied in MRI investigations. It is important to note that while these investigations have revealed numerous consequences, it is crucial to recognize that the findings may not universally apply to all individuals with ASD. Functional magnetic resonance imaging (fMRI) investigations primarily focus on examining the local and global connectivity patterns within the brain. In contrast, structural MRI studies commonly employ volumetric and morphometric analysis techniques to investigate any deviations or abnormalities in the structure of the brain.

The absence of a standardized test or tool [9] for the diagnosis of autism presents a significant challenge in achieving an accurate diagnosis. Physicians conduct behavioral observations of the children or inquire with the parents regarding the children's medical history. One of the two diagnostic methods utilized for the identification of autism is the autism diagnostic observation schedule (ADOS). This particular method places it is emphasis on the assessment of social interaction. The evaluator closely observes the individual under assessment and subsequently determines a grade based on their observations. During the assessment process for autism, the subject is subjected to observation, and the examiner assigns scores based on their observations. The autism diagnostic interview-revised (ADI-R) is a commonly utilized structured interview that involves gathering information from parents regarding the developmental history of the individual [10]. The diagnostic tools used in this context have an observational nature, which increases the likelihood of generating false-positive results. This is especially true for individuals with a range of mental health disorders. The examples that deserve special attention include cases involving psychotic patients [11], childhood-onset schizophrenia [12], attention-deficit hyperactivity disorder (ADHD) [12], and various other disorders. The pursuit of precise brain biomarkers and the automation of the identification process for ASD are essential goals in diagnostic procedures. These objectives aim to overcome the limitations associated with clinical tests.

Deep learning algorithms have demonstrated significant success in the field of image processing. As a result, there is a considerable amount of interest in leveraging these algorithms for the analysis of fMRI data. This study examines the challenges and potential applications of deep learning techniques in the analysis of fMRI data for the detection and classification of neurological disorders. To identify ASDs, researchers have examined fMRI data using various deep learning techniques, including convolutional neural networks (CNNs). CNNs are particularly effective as they utilize local spatial patterns and hierarchical representations of brain activity [13].

Research studies have demonstrated that CNN-based methods exhibit the capability to accurately classify ASDs by effectively identifying distinctive characteristics specific to ASDs. Recurrent neural networks (RNNs) have been employed for the estimation of time-varying brain activity associated with ASD. This is achieved by leveraging the RNN's ability to capture the inherent temporal dynamics present in fMRI data. RNNs have the capability to identify patterns that differentiate individuals with ASD from those with typical brain development. This is achieved by analyzing sequential information present in fMRI data. Autoencoders have been employed for reducing the complexity of fMRI data, facilitating the identification of significant features for ASD classification. The reduction of noise and excessive dimensionality observed in fMRI data facilitates the identification of patterns associated with ASD. Despite the promising outcomes, there are several challenges that need to be addressed before deep learning methods can be effectively employed for ASD identification using fMRI data [14], [15]. The motivation and contribution for this research is mentioned below.

− ASD has emerged as a significant public health concern due to its escalating prevalence. Efforts should be made to enhance the welfare of individuals affected by this condition through timely identification and effective treatment. One potential approach for accurately identifying ASD and advancing our understanding of its neurological underpinnings involves the application of deep learning techniques in the analysis of fMRI data [16]. The primary objective of this study is to facilitate the advancement of deep learning applications in neuroimaging by tackling challenges related to data quality, pre-processing, model interpretability, and restricted data accessibility. The objective of the study is to facilitate collaboration and facilitate the sharing of data within the industry. Ultimately, the utilization of deep learning techniques for fMRI data analysis in the context of ASD diagnosis holds promise for enhancing clinical outcomes and enhancing the quality of life for individuals affected by this disorder.

- In this paper an attribute feature graph approach is designed by using the stastical dependencies features that necessarily accomplish the diagnosis of ASD. In the first phase the features extracted are designed based on the fMRI data with each section that is developed as a graph, in the next-step the attribute feature graph layer learns the features of the node information of various nodes by ASD classification.
- The main objective of this study is to use fMRI data to create a classification model that can distinguish between individuals diagnosed with ASD.
- The proposed model utilizes a transfer learning technique to improve model design and enhance classification performance. The researchers conducted systematic testing on the autism brain imaging data exchange (ABIDE) dataset, demonstrating that the proposed model outperforms existing state-of-the-art techniques efficiently.

Advancements in deep learning have enabled the integration of various data types, including multimodal data [17], [18]. Several academic studies have shown the effectiveness of deep learning in addressing medical challenges, including the identification of Alzheimer's disease using MRI and PET data [19], [20]. Deep learning has demonstrated success in understanding complex patterns like functional connectivity, making it a valuable diagnostic tool [21]. Utilizing multiple voxels as inputs allows exploring complex associations among variables at a higher level, leading to discrimination between affected and healthy cohorts and proposing optimal diagnostic strategies [22]. According to Nie *et al.* [22], a method called transfer subspace learning via low rank and sparse representation (TSL_LRSR) was proposed for unsupervised domain transfer, demonstrating promising outcomes on visual domain adaptation tasks. Variants of low rank representation (LRR), such as multi-site adaption framework via low-rank representation (maLRR) [23] and multi-source domain adaptation (MSDA) and multi-view sparse representation (MVSR), have been employed for identifying ASD across multiple sites, enhancing the precision of ASD classification by mitigating data heterogeneity.

According to Zhang *et al.* [13], axial slices of T1-weighted (T1w) sMRI were used for detecting anomalies through a two-step approach, achieving high area under curve (AUC) scores with generative adversarial network (GAN) architecture. According to Tang *et al.* [17], self-attention modules in GAN architectures were investigated for detecting alzheimer's disease and brain metastases, leading to significant AUC values. The abnormal-to-normal translation generative adversarial network (ANT-GAN), a cycle generative adversarial network (CycleGAN)-based approach, was devised to generate medical images to distinguish healthy and abnormal scans. Our study presents a novel approach [20] for multi-site adaptation using fMRI and low-rank representation (LRR) decomposition, specifically the maLRR framework. The primary goal is to identify a shared LRR for data from multiple sites, mitigating distribution disparities between them. The non-oscillatory brain connectivity technique [23] has been proposed to distinguish between ASD subtypes based on resting-state functional magnetic resonance imaging (rs-fMRI) signal.

The research work in this paper is organized in four section, the first section deals with the background of ASD its challenges and the related work is written involving the existing techniques used involving various deep learning techniques. In the second section, the proposed methodology is designed for ASD diagnosis. In the third section the results are evaluated on the ABIDE dataset which further evaluated various performance metrics considered.

## 2.    METHOD

The proposed model involves constructing brain statistical dependencies for spectrum disorder (SD)-based classification, which includes network deployment, feature learning (feature extraction and classification). Currently, the statistical dependencies are built from pre-processed MRI data using correlation analyses. The framework deals with high-dimensional features and a limited sample size of MRI data. To address the issue of inappropriate features, the rank correlation coefficient is utilized to develop an input feature map, emphasizing the most relevant features. The feature extractor employs a primitive CNN model, where various prototypes are automatically learned to represent different categories. A generic prototype loss, based on cross-entropy, is designed to optimize the CNN feature extraction and prototypes. Classification is achieved by matching and estimating Euclidean distance. Additionally, domain adaptation is introduced to enhance model training. Figure 1 shows the proposed framework.

The statistical dependencies analysis method is evaluated to analyse pairwise correlations amongst the median value of the MRI data utilized in every brain region. The correlation is used to evaluate the length of MRI time-series. Each subject here is defined as $g_x(u), g_y(u) \in \beta^Z$. The average of the MRI signals for the brain section $x$ and $y$ at time period $u(u = 1,2, \dots, U)$. $Z$ and $U$ depicts the number regions of interest (ROIs). with total number of points respectively. Then $SD_{xy}$ is defined as given in (1). Here $g_x$ and $g_y$ depict the mean of the MRI signals in the brain section $x$ and $y$. An SD network is constructed using correlation-based methods by evaluating the Pearson correlation between the time-series of each pair of ROIs.

$$SD_{xy} = \frac{\sum_{u=1}^{U}(g_x(u)-g_x)(g_y(u)-g_y)}{\sqrt{\sum_{u=1}^{U}(g_x(u)-g_x)^2} * \sqrt{\sum_{u=1}^{U}(g_y(u)-g_y)^2}} \qquad (1)$$
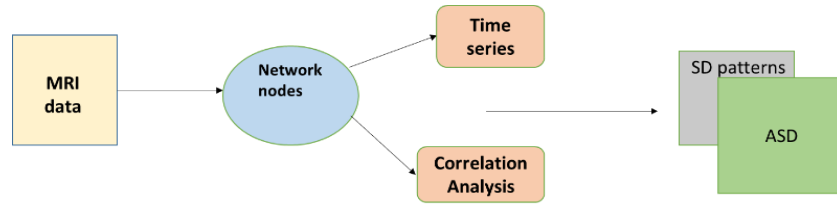


Figure 1. Proposed framework

## 2.1. Correlation estimation

The proposed framework utilizes rank correlation to generate input feature maps from high-dimensional MRI data samples. The feature ranking technique is critical for identifying crucial and pertinent MRI data and minimizing irrelevant data that slows down processing. To enhance $g_{xy}$ which denotes the $x-th$ statistical dependencies for the $y-th$ sample and the $h_y$ shows the sample's class label. The observation pairs shown here consists of the datasets $\{g_{xy}, h_y\}$ and $\{g_{xi}, h_i\}$ in in the distribution of (2). μ is a signum function, alternately $\{g_{xy}, h_y\}$ is in distribution of $\{g_{xi}, h_i\}$ where, shown as in (3). The correlation coefficient (**δ**) for the $x-th$ $SD$ is defined as in given (4). In the below equation $k_a$ and $k_b$ depicts the amount of distributions and pairs irrespective of the (2) and (3), $z$ and $l$ depicts how many samples were collected from the patient and control groups. The $SD$ is ranked in accordance with (δ), the input-feature map is projected by the proposed framework developed by the $SD$.

$$\mu(g_{xy} - g_{xi}) = \mu(h_y - h_i) \qquad (2)$$

$$\mu(g_{xy} - g_{xi}) = -\mu(h_y - h_i) \qquad (3)$$

$$\delta_x = \frac{k_a - k_b}{z * l} \qquad (4)$$

## 2.2. Proposed framework

The neural network automatically learns multi-level features from the input training data using filters and updates its parameters during the training process. In this research, a novel artificial neural network (ANN) integrated with the proposed framework for classifying the brain's functional network. The ANN here is employed through the feature extraction mechanism depicted as $h(g; \varphi)$, here $g$ denotes the input samples whereas $\varphi$ the parameters of ANN. In this model, the ANN consists of an input layer, three convolution layers, a max-pooling layer (2×2), a fully connected layer, and an output layer. The max-pooling layer is utilized for down-sampling and selecting values within local neighborhoods. The activation function $R$ is employed.

In the context of prototype learning, the output of the feature extraction step is utilized from both nodes. The prototypes for each class were created using the basic characteristics of the ANN in a fixed manner. This strategy introduces a novel technique in which prototypes are automatically learned for each category. The creation of each prototype begins by utilizing the initial prototype specific to its corresponding class. This initial prototype is developed based on the feature space derived from a pre-training set, which captures the characteristics present in each sample category. The distance between each sample and the current prototype is calculated by considering the adjacent prototypes at each sample. The attributes that have been identified through multiple prototypes associated with each category are subsequently utilized in the development of the subsequent prototype for that particular category. Here $U = \{u_{xy}|x = 1,2,……,G; y = 1,2,…..,I\}$ depicts the prototypes where $x \in \{1,2,……,G\}$ represents the index for the categories and $x \in \{1,2,……,I\}$ shows the prototype index for each category that is displayed. The model training involves, the feature extractor $h(g; \varphi)$, the prototypes as $\{u_{xy}\}$ are trained combined. For model training, a prototype loss function is used, which is based on distance-based cross-entropy. This loss function helps optimize the model by taking into account the differences between the prototypes and the training data. The distance-entropy generated during model training serves as the metric for measuring the similarity between samples and is utilized as the foundation for the loss function $(g, h)$ and the prototype $u_{xy}$.

$$p(h(g;\varphi), u_{xy}) = \| h(g;\varphi) - u_{xy} \| \tag{5}$$

The likelihood or probability of the sample $(g, h)$ the association or belongingness of the sample to the prototype. $u_{xy}$ can be estimated by $C(g \in u_{xy}|g) \propto -p(h(g;\varphi), u_{xy})$. To guarantee the non-negativity and the probability total as $C(g \in u_{xy}|g)$ is defined aa in (6). $\mu$ is a hyper parameter, through the probability $C(g \in u_{xy}|g)$ then $C(g|h)$ is defined as given in (7). The cross-entropy loss is defined as the negative log in accordance with the (8).

$$C(g \in u_{xy}|g) = \frac{\exp(-\mu p(h(g;\varphi), u_{xy})}{\sum_{o=1}^{B} \sum_{m=1}^{I} \exp(-\mu p(h(g;\varphi), u_{xy}))} \tag{6}$$

$$C(g|h) = \sum_{y=1}^{I} C(g \in u_{gy}|h) \tag{7}$$

$$loss((g, h); \varphi, U) = -log C(g|h) \tag{8}$$

To reduce the distance-based entropy the loss is decreased and the separation between the samples and the category prototype. The feature learnt is closer to the class in improvisation of intra-class concise, causing the feature representation to stand out. The prototype loss further lowers overfitting, improving generalizability in the process. The prototype loss is defined as in (9). Here $u_{gy}$ denotes the closest prototype for $h(g;\varphi)$ for the corresponding section $g$. The distance based-loss with the prototype to determine the total loss is mentioned in (10).

$$closs((g, h); \varphi, U) = ||h(g;\varphi) - u_{gy}||^2 \tag{9}$$

$$\begin{aligned} Total(((g, h); \varphi, U) \\ = loss((g, h); \varphi, U) + \vartheta\, closs((g, h); \varphi, U) \\ -log \sum_{y=1}^{I} \frac{\exp(-\mu p(h(g;\varphi), u_{xy})}{\sum_{o=1}^{B} \sum_{m=1}^{I} \exp(-\mu p(h(g;\varphi), u_{om}))} + \vartheta ||h(g;\varphi) - u_{gy}||^2 \end{aligned} \tag{10}$$

$\vartheta$ is the hyper-parameter for the $\varphi$ and the prototype are trained by minimising the loss function in (10). This is further computed in accordance with the error propagation algorithm and derive in regard with the updated parameters is determined by the chain rule. The optimization algorithm is employed for training the model for updating the framework. The number of iterations allowed throughout the training phase is set at 800., with initial learning fixed to 0.0001 for the hyper parameter $\vartheta$. Algorithm 1 is mentioned as follows.

Algorithm 1. Optimization algorithm
Step 1   $Dataset = \{(g_1, h_1), (g_2, h_2), \dots \dots, (g_k, h_k)\}$, loss denoted by $o$
Step 2   Initialization for the feature extraction $h(g;\varphi)$ and the prototypes $\{u_{xy}\}$
Step 3   While stopping criteria not meet do
Step 4   Sampling batch $u$ from $Dataset$
Step 5   Batch u sample into the proposed forward propagation
Step 6   The gradients evaluated are $\frac{do}{d\varphi}$ and $\frac{do}{u_{xy}}$ by back propagation and chain rule
Step 7   Update the value $\varphi$ and $\{u_{xy}\}$ the Adam optimization algorithm utilizes gradients, as per its formulation. $\frac{do}{d\varphi}$ and $\frac{do}{u_{xy}}$
Step 8   end while
Step 9   return updated model parameters $\varphi$ and $\{u_{xy}\}$

In the classification stage, the sample is classified based on prototype matching, and it is identified as belonging to the adjacent prototype through the calculation of Euclidean distance in the feature space. This process is defined as given in (11). Here $v_x(g)$ is the discriminant function in the section $x$, as mentioned in (12). The input pattern, represented as $g$ in abstract form, is compared to a number of prototypes, and the input sample is categorized according to the location of the neighboring prototype.

$$g \in sec\, argmin_{x=1}^{B} v_x(g) \tag{11}$$

$$v_x(g) = min_{y=1}^{I} ||h(g;\varphi)||^2 \tag{12}$$

## 2.3. Developing statistical dependencies features

Statistical dependencies features are constructed by assessing the similarity on the pre-processed data. The implementation procedure includes segmenting the brain into multiple divisions, and in the second step, the correlation coefficient is employed to estimate the correlation $A_{xy}$ amidst the brain segments $A_x$ and $A_y$. Finally, a correlation co-efficient matrix is determined for Z*Z matrix built for each subject. Here Z

denotes the ROI. The statistical dependencies matrix, is expressed as given in (13). Each row in the vector $j_a$ for the statistical dependencies matrix is selected for the SD features shown as in (14).

$$G = \begin{matrix} A_{11} & A_{12} & A_{1Z} \\ A_{21} & A_{22} & A_{2Z} \\ A_{Z1} & A_{Z2} & A_{ZZ} \end{matrix} \tag{13}$$

$$j_m = A_{m1}, A_{m2}, \ldots, A_{mz} \tag{14}$$

## 2.4. Attribute feature graph with self-attention mechanism layers

The integration of the attribute feature graph model with statistical dependencies features involves two segments. In the first section, an ROI is used as a node, and the statistical dependencies features extracted from the MRI data are combined into the graph. The connections linking the nodes in the graph, which reflect the characteristics of each subject, create the graph. The graph representation for each subject is denoted as $G = j, F$ here $b$ is the node feature set and $F$ The edges connect the two nodes in the graph. The second part deals with node features and the process of detecting ASD. Figure 2 shows the workflow of the proposed architecture.

- Designing an attribute feature graph: In this representation, each ROI is denoted as a node, The absolute number denotes the weight assigned to each edge as $A_{xy}$: $|A_{xy}|$, the edge set is expressed as: $F = |A_{11}|, |A_{12}|, \ldots, |A_{xy}|$, $x, y \in 1,110$. The designed feature-set for each row of statistical dependency is used as an attribute feature graph to generate $= j_1, j_2, \ldots, j_z \ldots, j_x \in \beta^{na}$, $na$. The node dimension depicts the attributes of each node. The attribute feature graph is built for each subject as $G = j, F$.

- Self-attention-based graph layers: this is developed for the purpose of learning node representation. Here the $Z$ value of attribute feature graph is fixed to 2. These node's input characteristics is $j = j_1, j_2, \ldots, j_z \ldots, j_x \in \beta^{na}$ and the output of the for the node characteristics, node-set $j' = j_1', j_2', \ldots, j_z' \ldots, j_x' \in \beta^{na'}$. A weight matrix $WM \epsilon \beta^{na'*na}$ trained amongst other nodes. The nodes are shown, and a self-attention process aggregates the nearby nodes for each node. The purpose of the attention coefficient is to:

$$k_{xy} = vWMj_x, WMj_y \tag{15}$$

Here $v: \beta^{na'} * \beta^{na'} \to \beta$ depicts the attention model which includes self-attention along with neighbourhood attention as $k_{xy}$ that depicts the significance of node $y$ to $x$. The softmax function denoted by is introduced that regularizes the neighbouring nodes denoted by $y \in Z_x$ of, as shown in (16). The attention mechanism $v$ is a neural network, $v \in \beta^{2na'}$. The sigmoid function in the output layer of the neural network is coupled to the weight matrix. The attention-based cross-correlation coefficient is obtained via (17). Here $trans$ depicts matrix transposition. The layers of the neural network, including the output layer's sigmoid function, are linked to the weight matrix. The attention-based cross-correlation coefficient is obtained shown as in (6). $\delta$ denotes the activation function and $y$ is traversed in $y \in Z_x$ denotes all nodes parallel to $x$ as given in (18).

$$n_{xy} = r\ k_{xy} = \frac{\exp k_{xy}}{\sum_{i \in Z_x} \exp k_{xy}} \tag{16}$$

$$n_{xy} = rsig k_{xy}$$
$$\frac{\exp sigvtrans[WMj_x||WMj_y]}{\sum_{i \in Z_x} \exp sigvtrans[WMj_x||WMj_i]} \tag{17}$$

$$j_x' = \delta[\sum_{y \in Z_x} n_{xy} WMj_y] \tag{18}$$
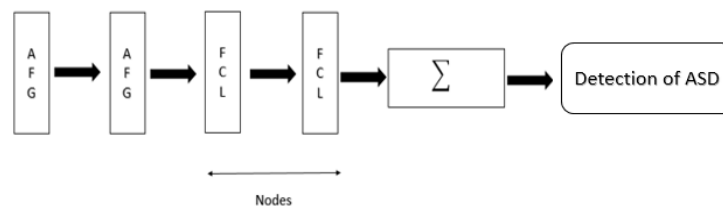


Figure 2. Workflow of the proposed architecture

**2.5. Attention mechanism**

An attention mechanism is built by the transformer attention mechanism. The features are learnt by this and they describe signals through various sides. The independent attention mechanisms are described in $I$ in (7), the nodes in feature representation depicts each attention to develop the final node representation, represented as given in (19).

$$j_x' = \underset{i=1}{\overset{I}{\|}} \delta[\sum_{y \in z_x} n_{xy}{}^I WM^I j_y] \tag{19}$$

Here I denote the attention heads, $I = 3$. $n_{xy}{}^I$ is the attention co-efficient estimated through the $I - th$ attention head with the size of $\frac{na'}{I} * na$. We immediate layer for node feature representing by each attention connection via the output dimension for $Ina'$. The attribute feature graph performs multiple attention mechanisms, $I$-th in the final layer, the attention-based cross-correlation coefficient is utilized instead of the operation to generate the final output, preserving the initial input dimension. Along with for allowing the application of the final non-linear function. The node feature representation in the final layer is depicted as given in (20). The attention mechanism updates the node $j_1$ representation in the neighborhood based on the calculated weights from the target node.

$$j_x' = \delta[\frac{1}{I}\sum_{i=1}^{I} \sum_{y \in z_x} n_{xy}{}^I WM^I j_y] \tag{20}$$

**3.    PERFORMANCE EVALUATION**

To assess the effectiveness of the proposed method, the study conducts inter-site cross-validation using data from 17 sites obtained from the ABIDE database. During the validation process, one site is designated as the testing target domain, while the remaining 16 sites act as multiple training source domains. This procedure is repeated multiple times, allowing each site to serve as the target domain to ensure the model's stability and generalizability in handling heterogeneous multi-site data.

**3.1. Dataset details**

The ABIDE collection comprises data from individuals diagnosed with ASD as well as individuals who exhibit typical development. The availability of this dataset enables researchers to conduct studies on the neurological foundations of ASD, owing to its comprehensive and diverse assortment of imaging and clinical data. The dataset comprises structural MRI, resting-state fMRI, and diffusion-weighted magnetic resonance imaging (dMRI) scans for each participant, along with accompanying clinical and demographic information. A comprehensive dataset comprising data from multiple imaging modalities and scanners has been generated through collaborative efforts from various research institutes worldwide. The ABIDE dataset is a valuable resource for researchers interested in exploring the connections between brain connectivity, structural abnormalities, and biomarkers associated with ASD. The utilization of this tool has been extensive in the enhancement and testing of machine learning and data-driven approaches for the diagnosis and description of autism. In this study, the ABIDE I dataset serves as the primary focus of analysis, encompassing information from a total of 1,102 participants.

**3.2. Comparison methods considered on the ABIDE dataset**

The suggested method's effectiveness is assessed by comparing the findings with those from different other disciplines, and the effectiveness is further demonstrated by experimental analysis. The ABIDE collection comprises data from individuals diagnosed with ASD as well as individuals who exhibit typical development. A comprehensive dataset comprising data from multiple imaging modalities and scanners has been generated through collaborative efforts from various research institutes worldwide.
− Correlation alignment (CORAL) [24]: the goal of the approach is to address domain shift by aligning the second-order statistics of the probability distribution in both the source and target domains.
− Joint distribution adaptation (JDA) [25]: concurrently adjusting the marginal and conditional distributions during dimensionality reduction narrows the distributional gap between domains, thus facilitating the learning of a new data feature representation.
− Transfer component analysis (TCA) [26]: the approach involves generating a cross-domain feature representation using feature dimensionality reduction and the greatest mean discrepancy to measure the distance between domains.
− Manifold embedded distribution alignment (MEDA) [27]: the employed approach utilizes manifold feature learning and dynamic distribution alignment techniques to assess the relative importance of the

marginal and conditional distributions. This enables the establishment of a domain-invariant classifier capable of handling variations across domains.

− Transfer subspace learning via low rank and sparse representation (TSL_LRSR) [28]: the proposed methodology incorporates the use of LRR to project data from two separate domains onto a shared subspace. This enables the extraction of domain-invariant characteristic representations, effectively addressing distributional disparities between the two domains.

− Centroid matching and local manifold self-learning (CMMS) [29]: this method aims to minimize the disparity in the conditional distribution between two domains by utilizing a local manifold self-learning strategy to effectively capture the inherent local manifold structure of the target domain samples. This involves adaptively identifying centroids in both domains, enabling the direct assignment of labels to the target domain data. In this study, potential optimization parameters are investigated within a specific set of values: 0.001, 0.01, 0.1, 1, 10, and 100. Notably, default parameters from the references are excluded from this search. The following section outlines the advanced multi-site techniques used in the comparative analyses for detecting ASD.

− maLRR [30]: the domain invariant representation of features is obtained using LRR. This involves extracting the shared component from specific projection matrices related to different source domains, which are then utilized as the reference domain's projection matrix.

− Denoising autoencoder [31]: the method involves reducing the dimensionality of the data by learning a domain-invariant feature representation unsupervisedly using two stacked denoising autoencoders.

− Deep belief network (DBN) [32]: this study employs a depth-first search methodology with a constrained route to investigate the topological information concealed within a graph. The selection of significant functional connection characteristics is accomplished through the utilization of a graph-based feature selection approach. Subsequently, an ASD identification process is carried out through the utilization of a three-tiered DBN that incorporates automated hyper-parameter modification.

− Autism spectrum disorder framework for diagnostic network (ASD-DiagNet) [33]: the utilization of autoencoder and single-layer perceptrons in combination with joint learning is employed to augment the precision The utilization of feature extraction enhances the model's parameters.

− Federated training and adversarial alignment approach (Fed_Align) [34]: This approach showcases the technique of utilizing the adversarial domain adaptation approach to depict domain-invariant characteristics.

### 3.3. Results

The results are evaluated for the proposed method for accuracy, sensitivity, specificity and recall and depicted in the form of graph for various existing state-of-art methods CORAL [24], JDA [25], TCA [26], MEDA [27], TSL_LRSR [28], CMMS [29], maLRR [30], denoising autoencoder [31], DBN [32], ASD-DiagNet [33], Fed_Align [34]. Table 1 shows the accuracy comparison for various state-of-art methods. From the accuracy evaluation, we can say that proposed system has better accuracy. In Figure 3, the accuracy comparison is carried out with various existing state-of-art methods. Where maLRR [30] generates a value of 59.9, TSL-LRSR [28] generates a value of 61.9, auto encoder [31] generates a value of 62.1, JDA [25] generates a value of 64.8. CORAL [24] generates a value of 64.9, TCA [26] generates a value of 65.7, DBN [32] generates a value of 68, DiagNet [33] generates a value of 68.8, MEDA generates a value of 69, CMMS [29] generates a value of 70, Fed_Align generates a value of 71.1, LRCDR [ES-existing system] generates a value of 73.1. Whereas PS depicts a value of 83.46 which gives better performance in comparison with existing system.
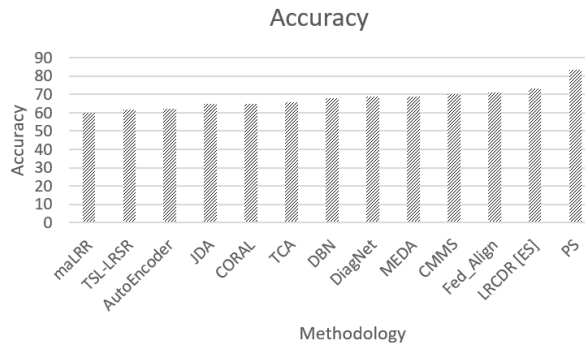
Table 1 Accuracy comparison

| Method | Accuracy |
|---|---|
| maLRR | 59.9 |
| TSL-LRSR | 61.9 |
| Auto Encoder | 62.1 |
| JDA | 64.8 |
| CORAL | 64.9 |
| TCA | 65.7 |
| DBN | 68 |
| DiagNet | 68.8 |
| MEDA | 69 |
| CMMS | 70 |
| Fed_Align | 71.1 |
| LRCDR [ES] | 73.1 |
| Proposed System (PS) | 83.46 |

Figure 4 shows the sensitivity metric comparison is carried out with various existing state-of-art methods. Where TSL-LRSR [28] generates a value of 36.4, maLRR [30] generates a value of 52.9, JDA [25] generates a value of 57.7, CORAL [24] generates a value of 59.7, Fed_Align generates a value of 64.3, Auto encoder [31] generates a value of 65.6, MEDA generates a valu e of 66.5. DiagNet [33] generates a value of 68.8TCA [26] generates a value of 66.9, CMMS [29] generates a value of 68, DBN [32] generates a value of 68.4, LRCDR [ES] generates a value of 71 whereas PS depicts a value of 81.24, which gives better performance in comparison with existing system. Table 2 shows the sensitivity comparison.

Figure 3. Accuracy comparison for various existing methods in comparison with proposed system
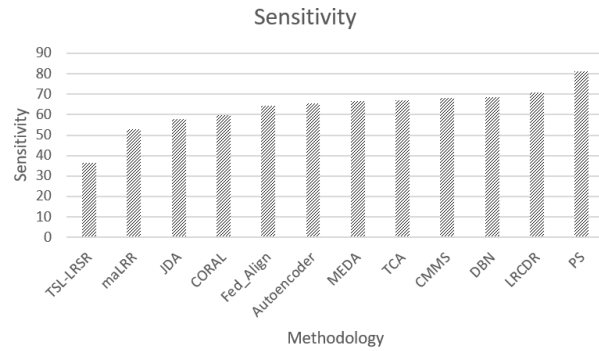
Figure 4. Sensitivity comparison for various existing methods in comparison with proposed system

Table 2. Sensitivity comparison

| Method | Sensitivity |
|---|---|
| TSL-LRSR | 36.4 |
| maLRR | 52.9 |
| JDA | 57.7 |
| CORAL | 59.7 |
| Fed_Align | 64.3 |
| Autoencoder | 65.6 |
| MEDA | 66.5 |
| DiagNet | 66.6 |
| TCA | 66.9 |
| CMMS | 68 |
| DBN | 68.4 |
| LRCDR | 71 |
| PS | 81.24 |

Figure 5 shows the specificity metric comparison is carried out with various existing state-of-art methods. Table 3 shows the specificity comparison. Table 4 show the F1-score comparison. Figure 6 shows the F1-score comparison graph. Where TSL-LRSR [28] generates a value of 36.4, maLRR [30] generates a value of 52.9, JDA [25] generates a value of 57.7, CORAL [24] generates a value of 59.7. Fed Align generates a value of 64.3, auto encoder [31] generates a value of 65.6, MEDA generates a valu e of 66.5, DiagNet [33] generates a value of 68.8TCA [26] generates a value of 66.9, CMMS [29] generates a value of 68. DBN [32] generates a value of 68.4, LRCDR [ES] generates a value of 71 whereas PS depicts a value of 81.24. Proposed system gives better performance in comparison with existing system.

## 2.4. Comparative analysis

The comparative analysis is carried out further in comparison with the existing system and proposed system for various performance metric is evaluated and the improvisation in % is shown in the Table 5. For Accuracy metric the ES generates a value of 73.1 and PS generates a value of 78.46 and the improvisation is 7.07311%. whereas for sensitivity metric the ES generates a value of 71 and PS generates a value of 81.24 and the improvisation is 13.5424%. For specificity metric the ES generates a value of 75.1, PS generates a value of 87.43%, and the improvisation is 15.1726% whereas for F-score metric, the ES generates a value of 73.8 and PS generates a value of 83.8 and the improvisation is 12.69045%.
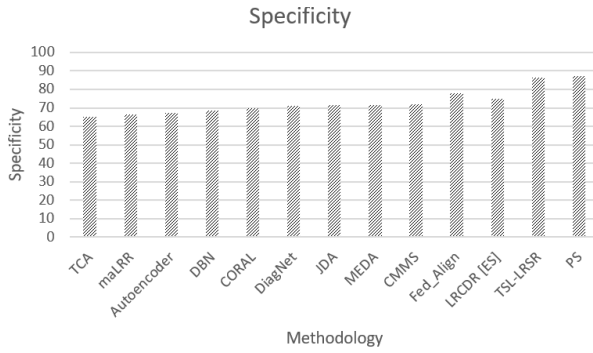
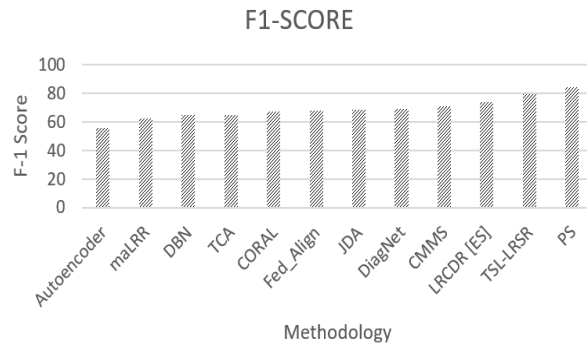Figure 5 Specificity comparison for various existing methods in comparison with proposed system



Figure 6. F1-score comparison for various existing methods in comparison with proposed system

Table 3. Specificity comparision

| Method | Specificity |
|---|---|
| TCA | 65.1 |
| maLRR | 66.3 |
| Autoencoder | 67.3 |
| DBN | 68.5 |
| CORAL | 69.8 |
| DiagNet | 71 |
| JDA | 71.4 |
| MEDA | 71.4 |
| CMMS | 72 |
| Fed_Align | 77.7 |
| LRCDR [ES] | 75.1 |
| TSL-LRSR | 86.2 |
| PS | 87.43 |

Table 4. F1-Score comparison

| Method | F1 |
|---|---|
| Autoencoder | 55.6 |
| maLRR | 62.5 |
| DBN | 64.4 |
| TCA | 64.6 |
| CORAL | 67.1 |
| Fed_Align | 67.8 |
| JDA | 68.3 |
| DiagNet | 68.7 |
| CMMS | 70.7 |
| LRCDR [ES] | 73.8 |
| TSL-LRSR | 79 |
| PS | 83.8 |

Table 5 Comparison table

| Performance metric | ES | PS | Improvisation (%) |
|---|---|---|---|
| Accuracy | 73.1 | 78.46 | 7.07311 |
| Sensitivity | 71 | 81.24 | 13.4524 |
| Specificity | 75.1 | 87.43 | 15.1726 |
| F-score | 73.8 | 83.8 | 12.69045 |

## 4. CONCLUSION

A deep learning model called the attribute feature graph layer has been developed for identifying individuals with ASD. The model utilizes an attribute feature graph for identification purposes. This graph is constructed by leveraging fMRI data to establish node characteristics. The learning process for node features involves establishing connections within the attribute feature graph between nodes and their corresponding attributes. The probability of ASD is determined by performing a weighted sum of the node features, which have been processed through the attribute feature network. Based on the analysis of brain functional

networks, this study proposes a framework for the classification of ASD. The framework integrates a customized CNN with experiential learning strategies. Transfer learning techniques are employed to enhance the convergence speed of models and optimize classification performance. The proposed model demonstrates improved performance in categorizing functional brain networks on large-scale datasets, as evidenced by rigorous testing conducted on the ABIDE dataset. Based on the conducted comparative analysis, the accuracy metric shows an improvement of 7.07311%, the sensitivity metric demonstrates an improvement of 13.4524%, the specificity metric exhibits an improvement of 15.1726%, and the F-score metric indicates an improvement of 12.69045%. These results suggest that our proposed model performs effectively when compared to the current system.

# REFERENCES

[1]  F. Ke, S. Choi, Y. H. Kang, K.-A. Cheon, and S. W. Lee, "Exploring the structural and strategic bases of autism spectrum disorders with deep learning," *IEEE Access*, vol. 8, pp. 153341–153352, 2020, doi: 10.1109/ACCESS.2020.3016734.
[2]  Z. Lu, J. Wang, R. Mao, M. Lu, and J. Shi, "Jointly composite feature learning and autism spectrum disorder classification using deep multi-output takagi-sugeno-kang fuzzy inference systems," *IEEE/ACM Transactions on Computational Biology and Bioinformatics*, vol. 20, no. 1, pp. 476-488, 2023, doi: 10.1109/TCBB.2022.3163140.
[3]  Z. A. Huang, Z. Zhu, C. H. Yau, and K. C. Tan, "Identifying autism spectrum disorder from resting-state fMRI using deep belief network," *IEEE Transactions on Neural Networks and Learning Systems*, vol. 32, no. 7, pp. 2847–2861, 2021, doi: 10.1109/TNNLS.2020.3007943.
[4]  Z.-A. Huang *et al.*, "Federated multi-task learning for joint diagnosis of multiple mental disorders on MRI scans," *IEEE Transactions on Biomedical Engineering*, vol. 70, no. 4, pp. 1137–1149, Apr. 2023, doi: 10.1109/TBME.2022.3210940.
[5]  M. Eni, I. Dinstein, M. Ilan, I. Menashe, G. Meiri, and Y. Zigel, "Estimating autism severity in young children from speech signals using a deep neural network," *IEEE Access*, vol. 8, pp. 139489–139500, 2020, doi: 10.1109/ACCESS.2020.3012532.
[6]  J. Han, G. Jiang, G. Ouyang, and X. Li, "A multimodal approach for identifying autism spectrum disorders in children," *IEEE Transactions on Neural Systems and Rehabilitation Engineering*, vol. 30, pp. 2003–2011, 2022, doi: 10.1109/TNSRE.2022.3192431.
[7]  S. Liang, A. Q. M. Sabri, F. Alnajjar, and C. K. Loo, "Autism spectrum self-stimulatory behaviors classification using explainable temporal coherency deep features and SVM classifier," *IEEE Access*, vol. 9, pp. 34264–34275, 2021, doi: 10.1109/ACCESS.2021.3061455.
[8]  F. Ke, S. Choi, Y. H. Kang, K.-A. Cheon, and S. W. Lee, "Exploring the structural and strategic bases of autism spectrum disorders with deep learning," *IEEE Access*, vol. 8, pp. 153341–153352, 2020, doi: 10.1109/ACCESS.2020.3016734.
[9]  M. R. Ahmed, Y. Zhang, Y. Liu, and H. Liao, "Single volume image generator and deep learning-based ASD classification," *IEEE Journal of Biomedical and Health Informatics*, vol. 24, no. 11, pp. 3044–3054, 2020, doi: 10.1109/JBHI.2020.2998603.
[10] F. Ke and R. Yang, "Classification and biomarker exploration of autism spectrum disorders based on recurrent attention model," *IEEE Access*, vol. 8, pp. 216298–216307, 2020, doi: 10.1109/ACCESS.2020.3038479.
[11] C. Xia *et al.*, "Dynamic viewing pattern analysis: Towards large-scale screening of children with ASD in remote areas," *IEEE Transactions on Biomedical Engineering*, vol. 70, no. 5, pp. 1622–1633, May 2023, doi: 10.1109/TBME.2022.3223736.
[12] M. N. A. Tawhid, S. Siuly, K. Wang, and H. Wang, "Automatic and efficient framework for identifying multiple neurological disorders from EEG signals," *IEEE Transactions on Technology and Society*, vol. 4, no. 1, pp. 76–86, Mar. 2023, doi: 10.1109/TTS.2023.3239526.
[13] Y. Zhang *et al*., "Predicting the Symptom Severity in Autism Spectrum Disorder Based on EEG Metrics," *IEEE Transactions on Neural Systems and Rehabilitation Engineering*, vol. 30, pp. 1898-1907, 2022, doi: 10.1109/TNSRE.2022.3188564.
[14] C. Han *et al.*, "GAN-based multiple adjacent brain MRI slice reconstruction for unsupervised Alzheimer's disease diagnosis," in *Computational Intelligence Methods for Bioinformatics and Biostatistics,* Cham: Springer, 2020, pp. 44–54, doi: 10.1007/978-3-030-63061-4_5.
[15] M. Kohli, A. K. Kar, and S. Sinha, "The role of intelligent technologies in early detection of autism spectrum disorder (ASD): A scoping review," *IEEE Access*, vol. 10, pp. 104887–104913, 2022, doi: 10.1109/ACCESS.2022.3208587.
[16] G. Wen *et al.*, "Graph self-supervised learning with application to brain networks analysis," *IEEE Journal of Biomedical and Health Informatics*, vol. 27, no. 8, pp. 4154–4165, 2023, doi: 10.1109/JBHI.2023.3274531.
[17] Y. Tang, D. Chen, H. Liu, C. Cai, and X. Li, "Deep EEG superresolution via correlating brain structural and functional connectivities," *IEEE Transactions on Cybernetics*, vol. 53, no. 7, pp. 4410–4422, Jul. 2023, doi: 10.1109/TCYB.2022.3178370.
[18] X. Li, N. C. Dvornek, J. Zhuang, P. Ventola, and J. S. Duncan, "Brain biomarker interpretation in ASD using deep learning and fMRI," in *Medical Image Computing and Computer Assisted Intervention-MICCAI 2018*, Cham: Springer, 2018, pp. 206–214, doi: 10.1007/978-3-030-00931-1_24.
[19] C. Han *et al.*, "MADGAN: unsupervised medical anomaly detection GAN using multiple adjacent brain MRI slice reconstruction," *BMC Bioinformatics*, vol. 22, pp. 1-20, 2021, doi: 10.1186/s12859-020-03936-1.
[20] L. Sun, J. Wang, Y. Huang, X. Ding, H. Greenspan, and J. Paisley, "An adversarial learning approach to medical image synthesis for lesion detection," *IEEE Journal of Biomedical and Health Informatics*, vol. 24, no. 8, pp. 2303–2314, Aug. 2020, doi: 10.1109/JBHI.2020.2964016.
[21] Q. Yao and H. Lu, "Brain functional connectivity augmentation method for mental disease classification with generative adversarial network," in *Pattern Recognition and Computer Vision*, Cham, Springer, 2019, pp. 444–455, doi: 10.1007/978-3-030-31654-9_38.
[22] G. Nie *et al.,* "An Immersive Computer-Mediated Caregiver-Child Interaction System for Young Children with Autism Spectrum Disorder," *IEEE Transactions on Neural Systems and Rehabilitation Engineering*, vol. 29, pp. 884-893, 2021, doi: 10.1109/TNSRE.2021.3077480.
[23] A. Sadiq, M. I. Al-Hiyali, N. Yahya, T. B. Tang, and D. M. Khan, "Non-oscillatory connectivity approach for classification of autism spectrum disorder subtypes using resting-state fMRI," *IEEE Access*, vol. 10, pp. 14049–14061, 2022, doi: 10.1109/ACCESS.2022.3146719.
[24] B. Sun, J. Feng, and K. Saenko, "Return of frustratingly easy domain adaptation," *Proceedings of the AAAI Conference on Artificial Intelligence*, vol. 30, no. 1, Mar. 2016, doi: 10.1609/aaai.v30i1.10306.

[25]  M. Long, J. Wang, G. Ding, J. Sun, and P. S. Yu, "Transfer feature learning with joint distribution adaptation," in *2013 IEEE International Conference on Computer Vision*, Dec. 2013, pp. 2200–2207, doi: 10.1109/ICCV.2013.274.

[26]  S. J. Pan, I. W. Tsang, J. T. Kwok, and Q. Yang, "Domain adaptation via transfer component analysis," *IEEE Transactions on Neural Networks*, vol. 22, no. 2, pp. 199–210, Feb. 2011, doi: 10.1109/TNN.2010.2091281.

[27]  J. Wang, W. Feng, Y. Chen, H. Yu, M. Huang, and P. S. Yu, "Visual domain adaptation with manifold embedded distribution alignment," in *Proceedings of the 26th ACM international conference on Multimedia*, Oct. 2018, pp. 402–410, doi: 10.1145/3240508.3240512.

[28]  Y. Xu, X. Fang, J. Wu, X. Li, and D. Zhang, "Discriminative transfer subspace learning via low-rank and sparse representation," *IEEE Transactions on Image Processing*, vol. 25, no. 2, pp. 850–863, Feb. 2016, doi: 10.1109/TIP.2015.2510498.

[29]  L. Tian, Y. Tang, L. Hu, Z. Ren, and W. Zhang, "Domain adaptation by class centroid matching and local manifold self-learning," *IEEE Transactions on Image Processing*, vol. 29, pp. 9703–9718, 2020, doi: 10.1109/TIP.2020.3031220.

[30]  M. Wang, D. Zhang, J. Huang, P. T. Yap, D. Shen, and M. Liu, "Identifying autism spectrum disorder with multi-site fMRI via low-rank domain adaptation," *IEEE Transactions on Medical Imaging*, vol. 39, no. 3, pp. 644–655, 2020, doi: 10.1109/TMI.2019.2933160.

[31]  A. S. Heinsfeld, A. R. Franco, R. C. Craddock, A. Buchweitz, and F. Meneguzzi, "Identification of autism spectrum disorder using deep learning and the ABIDE dataset," *NeuroImage: Clinical*, vol. 17, pp. 16–23, 2018, doi: 10.1016/j.nicl.2017.08.017.

[32]  Z. A. Huang, Z. Zhu, C. H. Yau, and K. C. Tan, "Identifying autism spectrum disorder from resting-state fMRI using deep belief network," *IEEE Transactions on Neural Networks and Learning Systems*, vol. 32, no. 7, pp. 2847–2861, 2021, doi: 10.1109/TNNLS.2020.3007943.

[33]  A. Fong, T. Eslami, F. Saeed, V. Mirjalili, and A. R. Laird, "ASD-DiagNet: A hybrid learning approach for detection of autism spectrum disorder using fMRI data," *Frontiers in Neuroinformatics*, vol. 13, pp. 1-11, 2019, doi: 10.3389/fninf.2019.00070.

[34]  X. Li, Y. Gu, N. Dvornek, L. H. Staib, P. Ventola, and J. S. Duncan, "Multi-site fMRI analysis using privacy-preserving federated learning and domain adaptation: ABIDE results," *Medical Image Analysis*, vol. 65, pp. 1-14, 2020, doi: 10.1016/j.media.2020.101765.

## BIOGRAPHIES OF AUTHOR

**Shabeena Lylath** 🔗 is currently working as assistant professor in HKBK College of Engineering, Bangalore, India, she earned his Bachelor of Engineering BE degree in ISE from Channabasaveshwara Institute of Technology, Tumkur, India in 2005. She obtained her master's degree in M.Tech. (CSE) from Akshaya Institute of Technology, Tumkur, India in 2015. Currently she is a research scholar at REVA University doing her Ph.D. in School of Computer Science and Engineering. She has an Experience of 10 years in teaching in Computer Science and Engineering. Her areas of interest are artificial intelligence and machine learning. She can be contacted at email: shabeenal_12@rediffmail.com.

**Laxmi B. Rananavare** 🔗 is currently working as associate professor School of Computing and Information Technology, REVA University, Bangalore, India. She has vast experience of more than 30 years in teaching in Computer Science and Engineering. Her research interests are: artificial intelligence, machine learning, and natural language processing. She is involved in research of applications of artificial intelligence. She has published many in national and international conferences and journals. She can be contacted at email: laxmib.rananavare@reva.edu.in.